C. R. Chimie 17 (2014) 717–724

Contents lists available at ScienceDirect

Comptes Rendus Chimie

www.sciencedirect.com

Full paper/Mémoire

Pt-doped semiconductive oxides loaded on mesoporous SBA-15 for gas sensing☆

Elena-Mihaela Seftel [a,b], Pegie Cool [b], Anita Lloyd-Spetz [c], Doina Lutic [a,*]

[a] Department of Materials Chemistry, Al. I. Cuza University of Iasi, Bvd. Carol I, No. 11, 700506, Iasi, Romania
[b] Laboratory of Adsorption and Catalysis, Department of Chemistry, University of Antwerp, Universiteitsplein 1, 2610 Wilrijk, Belgium
[c] Division of Applied Sensor Science, Department of Physics, Chemistry and Biology, Linköping University, 581 83 Linköping, Sweden

ARTICLE INFO

Article history:
Received 30 June 2013
Accepted after revision 28 October 2013
Available online 13 December 2013

Keywords:
SBA-15 modification
Wet impregnation
Indium and tin oxide
Platinum
H_2 and propene sensing

Mots clés :
SBA-15 modifiée
Imprégnation humide
Oxydes d'indium et d'étain
Platine
Détecteur de H_2 et de propène

ABSTRACT

SBA-15-based solids combining semiconductive oxides (Sn and In) and noble metal (Pt) were prepared by an incipient wet impregnation method in order to obtain materials for gas sensing. The materials were characterized by XRD, BET adsorption, SEM, and TEM. The BET analysis allowed obtaining details about the specific surface areas, pore size, and modifications due to the indium and/or tin oxides followed by the Pt deposition. XRD data revealed that In_2O_3 did not enter the mesopores of SBA-15, preventing also the entrance of the Pt nanoparticles in the mesopores. On the other hand, SnO_2 nanoparticles further doped with Pt could enter the mesoporous network, affording a SBA-15 material loaded with SnO_2 and very small Pt nanoparticles with high dispersion. Tablets obtained by pressing the modified SBA-15 were tested as sensitive materials for propene and hydrogen detection.

RÉSUMÉ

Des solides à base de silice mésoporeuse de type SBA-15, dopés à la fois avec des oxydes de type semi-conducteur (Sn et In) et d'un métal noble (Pt), ont été préparés par la voie d'imprégnation humide contrôlée (*Incipient Wet Impregnation* [IWI]), dans le but d'obtenir des matériaux sensibles pour la détection des gaz. L'étude des caractéristiques des matériaux préparés a été réalisée par DRX, adsorption BET et microscopies MEB et MET. L'analyse BET a permis d'étudier la surface spécifique, la taille et la structure des pores des matériaux ainsi que les modifications texturales induites par l'incorporation combinée d'oxydes d'indium et/ou d'étain et de platine. L'analyse DRX a révélé que les espèces d'In_2O_3 ne sont pas localisées à l'intérieur de la structure mésoporeuse de SBA-15, empêchant de ce fait l'introduction des nanoparticules de Pt dans les mésopores. Par ailleurs, il a été démontré que les particules de SnO_2 dopées ultérieurement avec du platine pouvaient être incorporées dans la structure mésoporeuse de SBA-15, permettant ainsi l'obtention d'un matériau composite à base de SBA-15 chargé en SnO_2, avec de minuscules nanoparticules de Pt hautement dispersées. Des pastilles de ces matériaux obtenus par pressage ont été testées en tant que matériaux sensibles pour la détection du propène et de l'hydrogène.

1. Introduction

Since the discovery of mesoporous silicates molecular sieves in 1992 [1], nanostructured mesoporous materials have attracted considerable attention because of their

☆ Thematic issue devoted to François Garin.

* Corresponding author.
E-mail addresses: seftel_elena@yahoo.com (E.-M. Seftel), pegie.cool@ua.ac.be (P. Cool), spetz@ifm.liu.se (A. Lloyd-Spetz), doilub@yahoo.com (D. Lutic).

1631-0748/$ – see front matter
http://dx.doi.org/10.1016/j.crci.2013.10.012

highly ordered pore structure and high surface area. A number of studies have been performed to modify the mesoporous materials in order to increase their potential applicability [2–7]. Mesoporous SBA-15 silica represents a promising oxide support for many catalysts, allowing the immobilization of various kinds of species acting as active sites with high dispersion. It has a hexagonal array of uniform tubular channels with free pore diameters in the range of 5–30 nm, much larger than those of MCM-41, allowing much lower internal diffusion resistance and thicker walls, making it more stable during thermal and hydrothermal operations. These structural properties makes SBA-15 a suitable candidate for the confined immobilization and growth of semiconductive oxide nanostructures [8,9]. For the development of semiconducting metal oxide gas sensors [10], efforts are focused on the research of mesoporous silica materials to improve the properties of metal oxide gas sensors.

Semiconductive oxides are widely used as sensing layers for gas detection, due to their high capacity to adsorb both oxygen and reducing species and catalyze chemical reactions on the oxide's surface [11–13]. The sensing mechanism for the detection of reducing gases is based on several modifications of the surface state, as the electrical conductivity of the layer, the voltage changes across a semiconductive layer, field effects, changes of mass, temperature, light absorption, emission or reflection, the layer's permittivity, vibration frequency of a quartz crystal, etc. [13,14]. Among these mechanisms of detection, electrical resistance changes are by far the most commonly and largely used in both scientific investigation of the sensing properties of the materials, and in practical, commercially available devices.

If reductive species such as hydrogen, hydrocarbons, carbon monoxide should be detected, the improvement of the sensing properties is important, for example, by using noble metals as doping catalytic active species in the advanced oxidation reactions [15,16]. Since the adsorption of the sensing species occurs on the surface, the improvement of the material's sensitivity is possible by using solids with high specific area [2,17].

The modification of the electrical resistance of a sensing layer consisting in a mixture of semiconductive and conductive material can be explained by the electronic transfers occurring at a so-called triple-phase boundary, a place where the semiconductive and conductive material meet at the atomic level with the gaseous sensed species. The semiconductive oxides are good adsorbents for the oxygen; several species of O^{n-} ions are formed ($n = 0.5, 1$ or 2) on the surface. The electrons involved in this process are extracted from the solid, generating a depletion region on the outer shell and inducing the formation of a thin space-charge region [18]. The semiconductive phase becomes poor in electrons and its electrical resistance increases to an important extent. When a reducing species appears in the proximity of the surface, its adsorption process occurs; several electrons are subtracted from the molecule and migrate to the solid, compensating the lack of electron induced by oxygen adsorption, canceling the charge generated by oxygen adsorption; thus, the reductive species is oxidized and subsequently eliminated by desorption from the surface. The electrical resistance value increases at values proportional to the amount of the reducing species. The more these triple-phase boundaries exist on the surface, the more efficient is electron transfer. Deng and Petric [19] approached the modeling method to prove the role of the material's porosity by defining the size of the triple-phase boundary (TPB) in a material containing a semiconductive oxide and a metal, concluding that the porous materials are suited for the generation of a high number of TPB. Moreover, the gas response also depends on the ratio between the thickness of the depletion layer and that of the bulk semiconductor; a high surface-to-volume ratio (in nanoparticles, for example) is favorable to the sensing mechanism, as detailed by Afzal et al. in a review [20]. The use of Pt in the formulation of the sensor is believed to be beneficial, due to its well-known high dissociative adsorption capacity of hydrogen and hydrogen-containing organic species, as well as for the generation of a large density of TPBs [21]. Thus hydrogen or hydrogen-containing molecules dissociate on the Pt surface whereby hydrogen atom or ions are formed. The formed hydrogen is known to spill over to the oxide and for example form OH groups [22] which change the resistivity of the metal oxide.

In the present work, we aim to synthesize and characterize several active mesoporous solids obtained by the incipient wet impregnation (IWI) of SBA-15 with indium and tin oxides and oxide mixtures thereof together with platinum. The materials were tested for the detection of hydrogen and propene, by measuring the changes of the electrical resistance values of the solids conditioned as pressed pastilles.

2. Experimental part

2.1. Synthesis of the mesoporous SBA-15 silica

SBA-15 was prepared by the method established by Stucky et al. [23,24] using tetraethylorthosilicate (TEOS) as a silica source and triblock copolymer P-123, $EO_{20}PO_{70}EO_{20}$ with average molar weight 5800 as a templating agent. The synthesis was performed in strong acid medium. The molar composition of the synthesis mixture was: 1 TEOS:5.87 HCl:194 H_2O:0.017 P123. The synthesis procedure comprised the dissolution of P123 (4 g) in 150 ml of 2 M HCl aqueous solution for 4–6 h, then TEOS (9.14 mL) was added and magnetic stirring was continued for 8 h at 45 °C. The suspension was subsequently aged statically for 15 h at 80 °C under reflux. The solid was recovered by filtration, quickly washed with deionized water, dried in air at room temperature overnight then at 80 °C for 6 h. The removal of the organic template from the pores was achieved by slow-rate calcination (1 °C/min) in ambient air at 550 °C for 6 h.

2.2. Metal oxide/Pt doping of SBA-15 silica

The incipient wetness impregnation method was chosen as the modification technique due to its higher efficiency in penetration [25–27] of the impregnating

precursors within the cylindrical wide pores of the SBA-15. Solutions of indium chloride hydrate, tin (II) chloride hydrate and an equimolar mixture thereof, and of hexachloroplatinic acid (H_2PtCl_6) were prepared using anhydrous ethanol as a solvent. The dissolved amount was 1 mmol In and Sn salts per 5 mL of solvent. One gram of calcined SBA-15 powder was heated for 2 h at 473 K and while still hot, the salt solution was poured quickly on the powder and the beaker was covered to avoid the powder to spread off due to the fast evaporation of ethanol. The procedure was repeated after the thermal decomposition of the precursor salts at 723 K (1°/min) for 4 h, and this treatment made the SBA-15 to end up in an oxide mass ratio of about 32%. Finally, impregnation with platinum was made, by dissolving 0.52 g of H_2PtCl_6 in ethanol, aiming at reaching a 25% Pt mass ratio to the initial SBA-15 silica. Ethanol was chosen for its reasonable capacity for dissolving salts and its less polar character in comparison with water, which made it suited to internal wetting of the inner space of SBA-15. A final calcination using the same procedure allowed decomposition of H_2PtCl_6 into metallic Pt. A high Pt content was chosen to obtain a material where Pt plays an important role in gas sensing, and the preparation procedure was chosen since it prevents sintering, associated with deactivation of the sensors [28].

2.3. Characterization methods

The diffraction patterns were obtained on a Shimadzu D6000 machine, in the range of 2 theta 5–70°, using Cu Kα radiation (λ = 1.5406 Å). BET (Brunauer, Emmett and Teller) analysis, which allows measuring the specific surface areas – S_{BET} (m^2/g) – was performed by ultrapure nitrogen adsorption experiments at 77 K, after sample activation by degassing for 2 h below 10^{-3} Torr at 473 K on a NOVA 2200e machine (Quantachrome Instruments, Boynton Beach, FL, USA). The pore-size distribution was determined from the adsorption branch of the isotherm using the BJH (Barrett–Joyner–Halenda) method. The total pore volume (TPV, cm^3/g) was calculated as the amount of nitrogen adsorbed at the relative pressure value of ca. 0.99.

The particle morphology was investigated using a LEO 1550 VP field-emission scanning electron microscopy (SEM). The TEM investigations were performed using an FEI Tecnai G2TF 20 UT field-emission microscope operated at 200 kV.

2.4. Sensing tests and experimental set-up

The SBA-15 modified with indium and/or tin oxide and Pt was used as a sensing material for the detection of reducing gas species. The powder was pressed to form pastilles, applying a 4tf pressure. The pastilles were cut in smaller pieces. Electrical contacts, 1 mm in diameter spots of Au with a layer thickness of 1500 Å, were applied on both sides of the layer, by the evaporation technique, using a shadow mask. The pastilles were then connected by welding Au wires, 50 microns, and inserted into the exposure cell [29]. The cell was heated at 623 K, at a 100 mL/min flow of synthetic air. The various gas environments in the cell were achieved by using a gas mixer system, equipped with automatic valves, connected to a computer able to define the gas flows, concentrations and time values for each step by using specific software. The modification of the electrical resistance values was monitored by a Keithley device every 4 s and registered by a computer.

3. Results and discussions

3.1. Characterization of the solids

Several active mesoporous solids were obtained by impregnation of SBA-15 with indium and tin oxides and oxide mixtures thereof together with platinum. The BET analysis allowed obtaining details about the specific surface areas, pore size and modifications due to the oxides and Pt deposition. The BET isotherms and the pore size distribution are displayed in Fig. 1.

A typical Type-IV isotherm with a H_1 hysteresis loop is observed for the pure SBA-15 material and a high surface area was measured (Table 1), suggesting the formation of a highly ordered two-dimensional hexagonal mesoporous structure [24]. The first increase in adsorption at a relative pressure $(p/p_0) < 0.1$ is due to the completion of a monolayer and the beginning of multilayer adsorption on the surface, while the second increase at $p/p_0 = 0.5–0.7$ arises from the capillary condensation in the mesopores

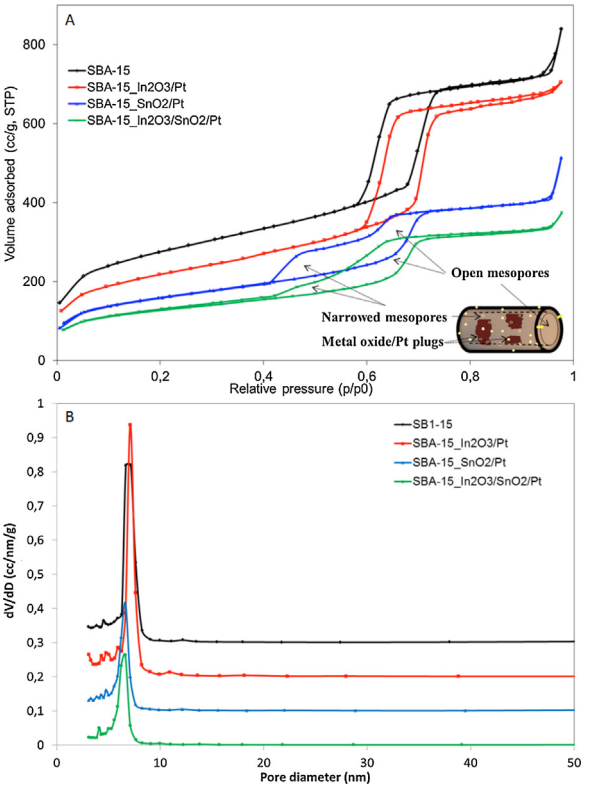

Fig. 1. (Color online) Changes in the (A) N_2-adsorption/desorption isotherms and (B) pore diameter of the pure and impregnated SBA-15 samples.

Table 1
Porosity characteristics of the obtained SBA-15-type samples.

Sample	[a]S_{BET} (m^2/g)	[b]TPV (cc/g)	[c]μS (m^2/g)	[d]μV (cc/g)	[e]D_p (nm)
SBA-15	883	1.137	225	0.143	7.153
SBA-15_In_2O_3/Pt	682	1.053	94	0.083	7.106
SBA-15_SnO_2/Pt	485	0.638	83	0.073	6.641
SBA-15_In_2O_3/SnO_2/Pt	382	0.524	74	0.063	6.621

TPV: total pore volume.
[a] BET surface area.
[b] Total pore volume.
[c] Micropore surface area.
[d] Micropore volume.
[e] Pore diameter.

with nitrogen multilayers adsorbed on the inner surface [30,31].

The isotherms for the impregnated samples show the characteristic behavior of ordered mesoporous SBA-15-type materials, indicating that the mesoporous structure is not disrupted after metal oxide/Pt loading. After impregnation with metal oxide/Pt nanoparticles, the surface area and total pore volume decreased (Table 1). The decrease in the surface area can be attributed to the partial filling of the mesopores and mostly the micropores. However, the isotherms for each of the obtained materials manifest particular characteristics, indicating differences in the pore shapes and sizes.

When loading with In_2O_3/Pt, the obtained material shows only a decrease in the specific surface area, with no obvious decrease of the pore dimensions. Moreover, the XRD data (discussed later in this section) showed the formation of very large In_2O_3 crystals together with small Pt nanoparticles, indicating that the In_2O_3 nanoparticles are located on the outer surface of the SBA-15 channels and are also inhibiting the insertion of the Pt nanoparticles into the mesopores of the SBA-15 material. This observation was also confirmed using the SEM technique used to analyze the morphology of the obtained material (see discussion in Fig. 3A).

A significant difference in the isotherm/hysteresis shape with a concomitant decrease in the specific surface area and pore size is observed when loading the SBA-15 material with SnO_2/Pt and the combination of the In_2O_3/SnO_2/Pt nanoparticles. In this case, the narrowing of the SBA-15 mesopores comes together with a significant reduction in the specific surface area. The presence of narrowed and blocked mesopores causes a delay in the evaporation of nitrogen from the pores, leading to a lower desorption relative pressure (p/p_0) and changes in the shape of the desorption branch of the isotherm. The observed effect on the isotherm shape and the interpretation as blocking or narrowing of the mesopores has also been described by other researchers [26]. Vansant et al. reported the formation of a Plugged Hexagonal Templated Silica (PHTS), an analogous of SBA-15, in which the silica nanoparticles inside the pores lead to the narrowing and the blocking of the SBA-15 mesopores.

The structure of the samples was investigated by XRD at wide angles. The patterns of the SBA samples modified with In, Sn and/or Pt are displayed in Fig. 2.

The XRD patterns show that the crystallization of the modification components occurs in very different ways for the three samples.

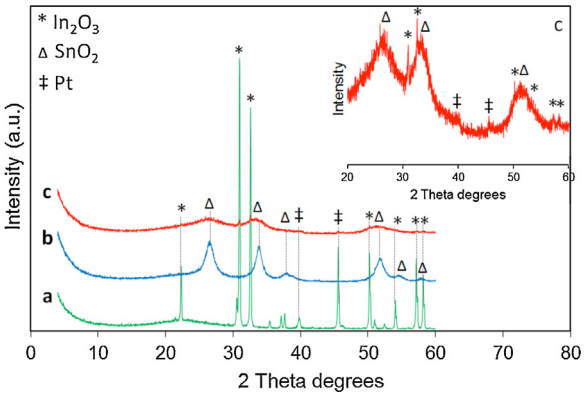

Fig. 2. (Color online) XRD patterns of (a) SBA-15_In_2O_3/Pt, (b) SBA-15_SnO_2/Pt and (c) SBA-15_In_2O_3/SnO_2/Pt samples. For clarity, the enlargement of pattern (c) is presented in the inset picture.

The degree of In_2O_3 crystallization for the sample SBA-15_In_2O_3/Pt is very high, since the mean peaks characteristic for the indium oxide appearing at 22.3°, 31°, 32.6°, 45.6°, 50.2° and 58° (2 theta), corresponding to the (211), (222), (400), (431), (440) and (622) plans [32–35] are very sharp, well defined, and intense. This could also be an evidence of the fact that indium oxide did not enter the mesopores of SBA-15, but formed a distinctive phase mechanically mixed between the SBA rods. The crystallite size of the observed In_2O_3 phase, calculated using the Scherrer equation [36,37] and selecting the (222) crystal plane, is 51.1 nm, indicating furthermore that the In_2O_3 nanoparticles could not easily enter the mesopores of the SBA-15 material. The peaks corresponding to the Pt phase are, as expected, a lot less intense and are located at 39.9° and 46°, respectively, in line with the values mentioned in references [38,39].

For the sample SBA-15_SnO_2/Pt, the five major peaks belonging to the SnO_2 phase appear at 26.8°, 34°, 38°, 52° and 55°; they were assigned, respectively, to the planes (110), (101), (200), (211), and (220) [40,41]. The crystallite size of the observed SnO_2 phase, calculated using the Scherrer equation [36,37] and selecting the (110) crystal plane, is 5.3 nm. Therefore, taking into account the calculated pore diameter (Table 1), it may be concluded that the SnO_2 nanoparticles are located inside the mesoporous channels of the SBA-15 material, leading to the narrowing of the mesopores, like also observed with the N_2-sorption technique. It should be mentioned that the peaks due to platinum are not present in the XRD pattern, probably due to the low nanoparticle size and its high dispersion [42].

The SBA-15_In_2O_3/SnO_2/Pt sample displays the same shape, but the peak heights are even lower than for the SBA-15_SnO_2/Pt sample. The magnification of the pattern (inset in: Fig. 2) shows two small peaks at 31° and 32.5°, belonging to the (222) and (400) planes of In_2O_3. For these two samples, the peaks corresponding to Pt are very weak. As mentioned above, the low intensity and the large peak weight are an indication of the small size of the particles. The absence of the platinum peaks in the case of the two mentioned samples indicates that the metal entered the

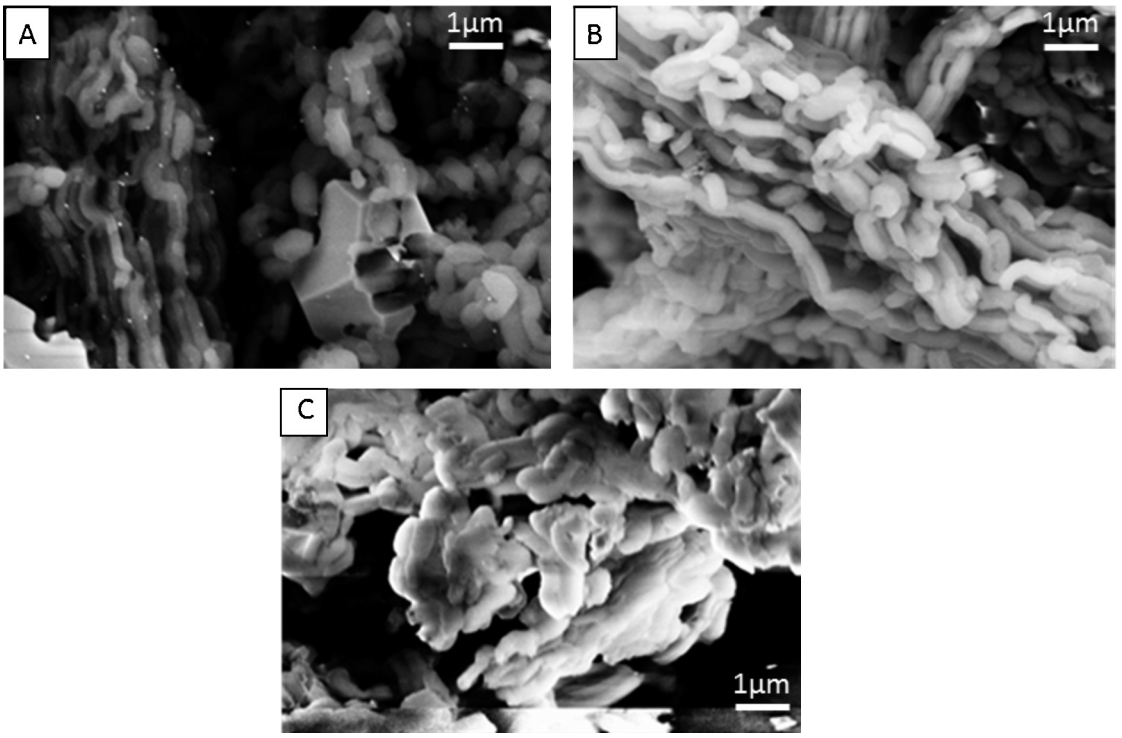

Fig. 3. SEM images of (A) SBA-15_In_2O_3/Pt, (B) SBA-15_SnO_2/Pt and (C) SBA-15_In_2O_3/SnO_2/Pt samples.

mesopores, in contrast to the case of the sample SBA-15_In_2O_3/Pt, where it seems that the indium oxide not only did not enter the pores, but also hindered the entrance of platinum inside the pores.

SEM analysis correlates well with the aspects already commented in the previous paragraphs; the images showing the morphology of SBA-15_In_2O_3/Pt, SBA-15_SnO_2/Pt and SBA-15_In_2O_3/SnO_2/Pt are presented in Fig. 3. Indium oxide segregates alone in large, polyfaceted crystals, while platinum appears as small individual bright particles in the case of SBA-15_In_2O_3/Pt (Fig. 3A). For the other two samples, the relative uniform rod-like morphology characteristic to SBA-15 is well preserved, without any evidence of deposition of other phases on the outer surface of the SBA-15 rods (Fig. 3B, C). This observation is well correlated with the conclusions withdrawn from the N_2-sorption and XRD techniques, Figs. 1 and 3. Pt nanoparticles are observed only for the SBA-15_In_2O_3/Pt sample, in both XRD patterns (Fig. 2a) and SEM (Fig. 3A). Their location on the outer surface of the SBA-15 channels is supported by N_2 sorption data (Fig. 1, red isotherm). For the other two samples, the Pt nanoparticles cannot be seen neither in the SEM images (Fig. 3B, C) nor in the XRD patterns (Fig. 2b, red and blue curves); this is an extra reason to assume the small size and high dispersion of the metal oxides/Pt nanoparticles in the mesopores of the SBA-15 matrix.

The TEM analysis of sample SBA-15_SnO_2/Pt indicates that some of the tin oxide is present on the outer surface of the SBA-15, which preserves its multi rod-like structure. The amount of platinum on the outer surface is quite low, indicating its high dispersion and its location inside the mesopores. This material is thus a good candidate as a sensing layer for gas species (Fig. 4).

3.2. Sensing properties

The sensing properties of samples SBA-15_SnO_2/Pt and SBA-15_In_2O_3/SnO_2/Pt at a temperature of 623 K were investigated for hydrogen detection in air. The volume ratio concentrations were 1%; 0.8%; 0.6%; 0.5%; 0.4%; 0.3%; 0.2%, and 0.1% hydrogen in air, respectively. A gas flow rate of 100 mL min^{-1} flowed on the sensing surface, at a constant temperature of 350 °C, normally for 30 min, followed by a pure air purge of 30 min (the exposure time was 60 min for the exposure to 0.8% H_2). The time dependence of the resistance value of the pastille is displayed in Fig. 5.

The material is sensitive to hydrogen in the investigated concentration range, showing a different response at different gas concentrations and a quite fast response. The fast response is usually accredited to the synergistic effect between the semiconductive oxide and the conductive Pt, which generates triple-phase boundaries that are very efficient in the electron transfer from the metal to the oxide framework. The noisy signal and the baseline variation are probably due to the imperfect electrical contacts between the metal contacts and the pastille and/or the bonding wires.

In order to investigate further the detection of lower concentrations of hydrogen, the sample SBA-15_SnO_2/Pt was exposed to 1000, 800 and 600 ppm of hydrogen; the

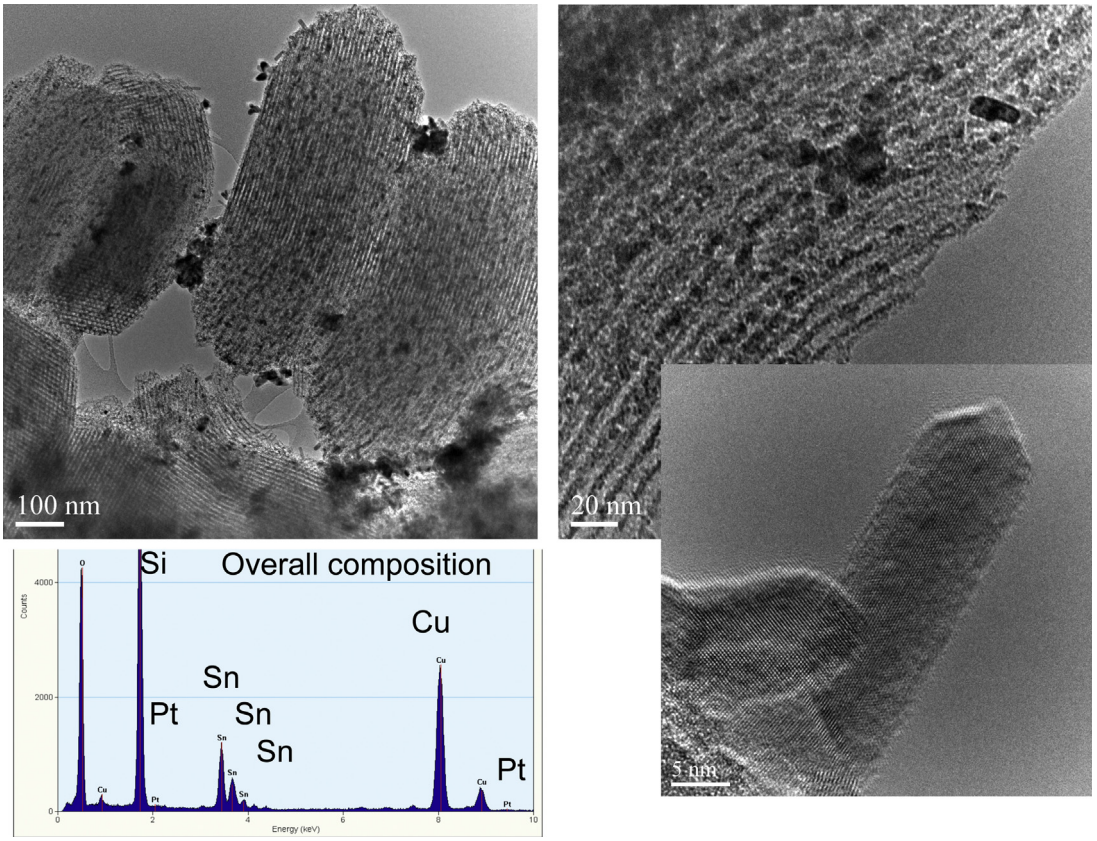

Fig. 4. (Color online) TEM analysis of the SBA-15_SnO_2/Pt sample. The EDAX insets show, respectively, the overall composition of the studied sample.

results are displayed in Fig. 6. The detection is also possible and quite fast responding, although the magnitude of the signal is not very high. It means the material is well responding to hydrogen in a wide concentration range in air.

The propene sensing tests (Fig. 7) were performed in the same experimental conditions, at concentrations of 240, 200, 150 and 100 ppm propene in air.

The signal for propene sensing is unexpectedly weak in comparison with that due to hydrogen. While the

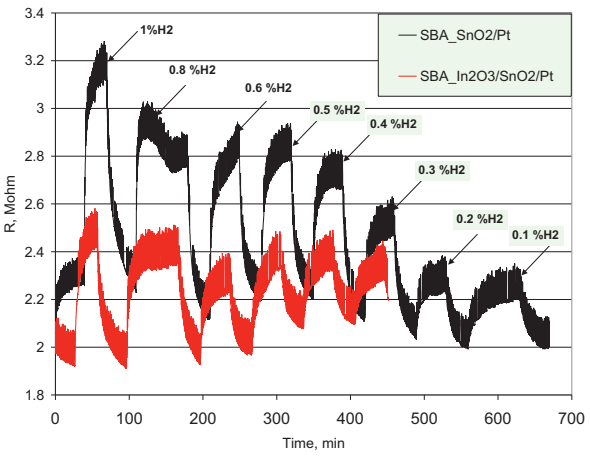

Fig. 5. (Color online) Resistance value of the sensing layer at different hydrogen concentrations in air.

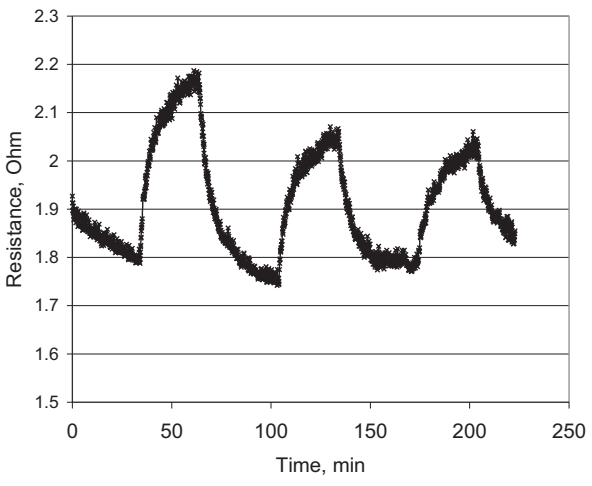

Fig. 6. Sensing tests at low hydrogen concentrations, 1000, 800, 100 ppm (sample SBA-15_SnO2/Pt, 350 °C).

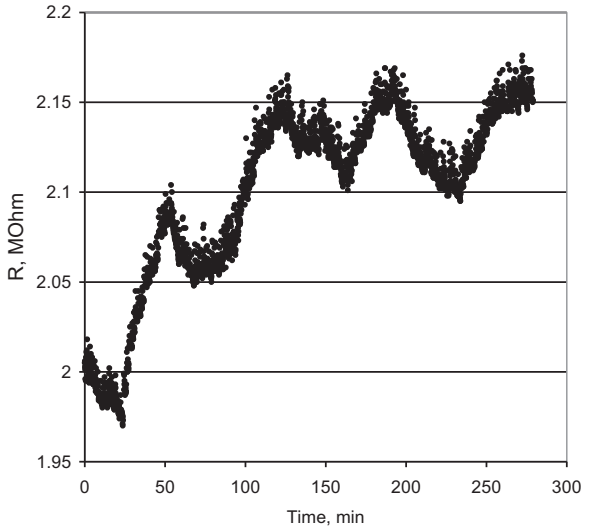

Fig. 7. Sensing tests for propene detection, 240, 200, 150, 100 ppm in air (sample SBA-15_SnO_2/Pt, 350 °C).

hydrogen molecule splits easily on the Pt sites or even on the semiconductive oxide and the oxidation is also very simple, with no co-products, the oxidation of propene involves a high number of participants like the adsorbed O_{ads}^{2-} species and a high number of holes from the surface, as shown by Sahner et al. [43]:

$$(4n+m)h^+ + (2n+m/2)O_{ads}^{2-} + C_nH_m \rightarrow nCO_2 + m/2H_2O$$

The number of available holes depends on the solid structure. In the case of a film deposited by the casting technique, as in our previous paper [44], the packing of the doped SBA-15 rods is very soft and the inner volume of the mesopores is easily accessible for the diffusion of the propene molecule. In the case of compressed pastilles conditioning used in this work, the packing of the solid particles is a lot more compact, so the diffusion of propene to the mesopores is partly hindered and the signal will be weakened. The close packing of the solid pressed in pastilles is also proved by the values of the intrinsic electrical resistance of the pressed tablets, which are of the order of the MΩ, higher by three of fours orders of magnitude than that of a film deposited by nanocasting [44]. The modifications due to propene oxidation cannot reach a high level in this range of solid electrical resistances. The baseline for propene sensing is established at 2.1 MΩ only after two exposure cycles. We assume that the propene molecules adsorbed on the strong adsorption sites could not be oxidized and that those sites became inactive for the subsequent exposures. The noisy signal and baseline indicate that, in this experimental set-up, the material is not an option for potential applications for propene sensing.

4. Conclusions

The incipient wet impregnation of SBA-15 with indium and tin oxides and Pt was performed to obtain nanoporous materials useful in the gas sensor formulation. The materials were structurally characterized by BET adsorption, XRD, SEM and TEM techniques. Indium oxide was admitted inside the SBA-15 pores to a big extent, while the tin oxide location determined the narrowing of the SBA-15 channels entering. The Pt particles sizes depended on the oxide species deposited simultaneously: indium determined the separated crystallization of big-size grains, visible in SEM and XRD, while the presence of tin, alone or with indium, determined a high dispersion of very small Pt particles, located both inside the mesopores of SBA-15 and on its external surface. The materials in the form of pressed pastilles were tested as sensing materials for hydrogen and propene, based on resistive measurements. The SBA-15_SnO_2/Pt solid was satisfactory sensitive towards hydrogen in the concentration range of 0.1–1% vol. in air, while the response toward ppm-range concentrations of propene was weak.

Acknowledgements

We kindly acknowledge the financial support for this work by MNT Era Net project SootSens II, No. 09044, MNT 7-028/2010 granted by CNMP – Romania. E. M. Seftel greatly acknowledges the Fund for Scientific Research – Flanders (FWO – Vlaanderen) for financial support. Performing of TEM analysis is acknowledged to Dr. Jose Manuel Cordoba.

References

[1] C.T. Kresge, M.E. Leonowicz, W.J. Roth, J.C. Vartuli, J.S. Beck, Nature 359 (1992) 710.
[2] G.E. Fryxell, Inorg. Chem. Commun. 9 (2006) 1141.
[3] P. Shah, A.V. Ramaswamy, K. Lazar, V. Ramaswamy, Appl. Catal. A Gen. 273 (2004) 239.
[4] I. Fechete, B. Donnio, O. Ersen, T. Dintzer, A. Djeddi, F. Garin, Appl. Surf. Sci. 57 (2011) 2791.
[5] A. Boulaoued, I. Fechete, B. Donnio, M. Bernard, P. Turek, F. Garin, Micropor. Mesopor. Mat. 155 (2012) 131.
[6] I. Fechete, O. Ersen, F. Garin, L. Lazar, A. Rach, Catal. Sci. Technol. 3 (2013) 444.
[7] S. Haddoum, I. Fechete, B. Donnio, F. Garin, D. Lutic, C. Eddine Chitour, Catal. Commun. 27 (2012) 141.
[8] M. Santhosh Kumar, D. Chen, A. Holmen, C. John, Walmsley, Catal. Today 142 (2009) 17.
[9] E.M. Seftel, P. Cool, A. Lloyd-Spetz, D. Lutic, J. Porous Mat. 20 (2013) 1119.
[10] S. Ashraf, C.S. Blackman, R.G. Palgrave, I.P. Parkin, J. Mater. Chem. 17 (2007) 1063.
[11] S.M. Kanan, O.M. El-Kadri, I.A. Abu-Yousef, M.C. Kanan, Sensors 9 (2009) 8158.
[12] K. Wetchakun, T. Samerjai, N. Tamaekong, C. Liewhiran, C. Siriwong, V. Kruefu, A. Wisitsoraat, A. Tuantranont, S. Phanichphant, Sens. Actuators B 160 (2011) 580.
[13] D. Lutic, A. Lloyd Spetz, M. Sanati, in: J.A. Rodriguez, M. Fernández-García (Eds.), Synthesis Properties and Applications of Oxide Nanomaterials, John Wiley & Sons, New York, 2007, pp. 411–450.
[14] B. Pejcic, P. Eadington, A. Ross, Environ. Sci. Technol. 41 (18) (2007) 6333.
[15] V. Aroutiounian, Int. J. Hydrogen Energy 32 (2007) 1145.
[16] T. Hubert, L. Boon-Brett, G. Black, U. Banach, Sens. Actuators B 157 (2011) 329.
[17] E. Comini, Anal. Chim. Acta 568 (2006) 28.
[18] A. Tiburcio-Silver, A. Sanchez-Juarez, Mat. Sci. Eng. B 110 (2004) 268.
[19] X. Deng, A. Petric, J. Power Sources 140 (2005) 297.
[20] A. Afzal, N. Cioffi, L. Sabbatini, L. Torsi, Sens. Actuators B 171–172 (2012) 25.
[21] V.M. Janardhanan, V. Heuveline, O. Deutschmann, J. Power Sources 178 (2008) 368.

[22] I. Lundström, H. Sundgren, F. Winquist, M. Eriksson, C. Krantz-Rülcker, A. Lloyd Spetz, Sens. Actuators B 121 (2007) 247.
[23] D. Zhao, Q. Huo, J. Feng, B.F. Chmelka, G.D. Stucky, J. Am. Chem. Soc. 120 (14) (1998) 2317.
[24] D. Zhao, J. Feng, Q. Huo, N. Melosh, G.H. Fredrickson, B.F. Chmelka, G.D. Stucky, Science 279 (1998) 548.
[25] Z. Lu, S. Ji, H. Liu, C. Li, Chin. J. Chem. Eng. 16 (5) (2008) 740.
[26] M. Bowker, A. Nuhu, J. Soares, Catal. Today 122 (2007) 245.
[27] S. Mahmoodi, M.R. Ehsani, S.M. Ghoreishi, J. Ind. Eng. Chem. 16 (2010) 923.
[28] M. Nishibori, W. Shin, K. Tajima, L.F. Houlet, N. Izu, T. Itoh, I. Matsubara, J. Eur. Ceram. Soc. 28 (2008) 2183.
[29] R.B. Bjorklund, S. Jaras, U. Ackelid, C.U.I. Odenbrand, L.A.H. Andersson, J.G.M. Brandin, J. Catal. 128 (1991) 574.
[30] F. Rouquerol, J. Rouquerol, K.S.W. Sing, Adsorption by Powders and Porous Solids Principles Methodology and Applications, Academic Press, London, 1991p. 441.
[31] E. van Bavel, P. Cool, K. Aerts, E.F. Vansant, J. Porous Mat. 12 (2005) 65.
[32] W.S. Seo, H.H. Jo, K. Lee, J.T. Park, Adv. Mater. 15 (10) (2003) 795.
[33] T. Sreethawong, S. Chavadej, S. Ngamsinlapasathian, S. Yoshikawa, Micropor. Mesopor. Mater. 109 (2008) 84.
[34] Z. Zhan, D. Jiang, J. Xu Mat. Chem. Phys. 90 (2005) 250.
[35] J. Buha, I. Djerdj, M. Niederberger, Cryst. Growth Design 7 (1) (2007) 113.
[36] E.M. Seftel, E. Popovici, M. Mertens, G. Van Tendeloo, P. Cool, E.F. Vansant, Micropor. Mesopor. Mater. 111 (2008) 12.
[37] Z. Chang, D.G. Evans, X. Duan, C. Vial, J. Ghabaja, V. Prevot, M. De Roy, C. Forano, J. Solid State Chem. 178 (2005) 2766.
[38] X. Zhang, K.Y. Chan, Chem. Mater. 15 (2003) 451.
[39] G. Neri, A. Bonavita, G. Rizzo, S. Galvagno, N. Pinna, M. Niederberger, S. Capone, P. Siciliano, Sens. Actuators B 122 (2007) 564.
[40] J. Zhao, W. Wang, Y. Liu, J. Ma, X. Li, Y. Du, G. Lu, Sens. Actuators B 160 (2011) 604.
[41] J. Yang, K. Hidajat, S. Kawi, Mater. Lett. 62 (2008) 1441.
[42] J. Tu, N. Li, X. Lai, Y. Chi, Y. Zhang, W. Wang, X. Li, J. Li, S. Qiu, Appl. Surf. Sci. 256 (2010) 5051.
[43] K. Sahner, R. Moos, M. Matam, J.J. Tunney, M. Post, Sens. Actuators B 108 (2005) 102.
[44] E.M. Seftel, P. Cool, D. Lutic, A. Lloyd-Spetz, J. Porous Mat. 20 (5) (2013) 1119.